A Novel Dynamic Channel Map for 6G MIMO Communications

Tianrun Qi[1], Chen Huang[2,1*], Jiayue Shi[1], Junling Li[1,2], Shuaifei Chen[2,1], and Cheng-Xiang Wang[1,2*]
[1]National Mobile Communications Research Laboratory, School of Information Science and Engineering, Southeast University, Nanjing 210096, China.
[2]Purple Mountain Laboratories, Nanjing 211111, China.
Email: tr_qi@seu.edu.cn, huangchen@pmlabs.com.cn, {jiayueshi, junlingli, shuaifeichen, chxwang}@seu.edu.cn

2024 IEEE/CIC International Conference on Communications in China (ICCC) | 979-8-3503-7841-2/24/$31.00 ©2024 IEEE | DOI: 10.1109/ICCC62479.2024.10682005

***Abstract*—The sixth generation (6G) wireless communication systems significantly increase the number of devices, antennas, and service nodes, bringing great demands on the accuracy and time-efficiency of 6G channel model. However, conventional channel modeling methods including deterministic and stochastic channel model cannot meet the accuracy and time-efficiency simultaneously. To solve this problem, we propose a novel stochastic-deterministic hybrid channel model, named dynamic channel map (DCM). By considering the mapping relationship between physical environment features and electromagnetic propagation mechanisms, the DCM can provide dynamic channel information and channel characteristics within a specific communication scenario. Furthermore, we compare the proposed channel model with deterministic channel model and stochastic channel model based on channel measurement. The results illustrate that the synthetic channel accords well with measurement channel, verifying the accuracy of DCM. Finally, the time cost on updating DCM is much less than conventional channel map construction methods, demonstrating the time-efficiency of DCM.**

***Index Terms*—6G, stochastic-deterministic hybrid channel model, dynamic channel map, accuracy and time-efficiency, channel measurement.**

I. Introduction

With the tremendous growth in mobile device connectivity and the continuous changes of the communications environment, the diversity of network service scenarios and the complexity of network control in 6G systems will far exceed those of the existing networks [1], [2], which brings great challenges to 6G channel model on accuracy and time-efficiency. Conventional channel model can be divided into deterministic channel model and stochastic channel model [3]. For deterministic channel model, ray tracing (RT) algorithms are widely used. RT is an electromagnetic field strength prediction algorithm based on geometric optics and consistency diffraction theory [4]. However, due to the large time-consuming, the RT channel model cannot support real-time and localized calibration. As for stochastic channel model, geometric-based stochastic channel modeling (GBSM) are commonly used for more accurate channel modeling in specific communication scenarios [5]–[7]. In [5], a 6G pervasive channel model (6GPCM) is proposed to characterize statistical properties of channels at all frequency bands from sub-6 GHz to visible light communication bands and all scenarios. However, GBSM only targets specific scenarios or limited link channel modeling. Although they consider the impact of scatterers in physical environment, GBSM in particular positions is still not accurate enough for 6G demands due to the randomness.

On the other hand, with the emergence of 6G, relying solely on instantaneous channel measurements will swiftly deplete available spectrum resources, hindering the sustainable development of 6G multiple-input multiple-output (MIMO) wireless communications. An accurate and time-efficient channel model can provide real-time CSI for pilot overhead reduction and trasmission optimization, further enhancing system performance and ensuring effective spectrum management. As an important concept and tool, channel map has attracted extensive academic attention and research. Channel map provides a detailed description of the wireless communication environment and channel characteristics within a specific geographic area. It includes critical data such as received signal strength, parameters of multipath components (MPC), and interference distribution. Channel map can be constructed based on channel model, storing the channel information and channel characteristics. Existing studies on channel map include channel knowledge map (CKM) [8]–[10] and radio environment map (REM) [11]–[14]. Among these studies, instantaneous channel measurement [13], RT method [11], and GBSM [5] are three main methods for channel map construction, all having their limitations discussed above in 6G MIMO communication systems.

From the literature, conventional channel model are either excessively time-consuming, e.g., RT, or inaccurate, e.g., GBSM, limiting their adoption in 6G dynamic wireless networks. In this paper, a novel DCM constructed by a stochastic-deterministic hybrid channel model are proposed, with the ability of providing accurate and time-efficient channel information and channel characteristics. The main contributions of this paper can be summarized as follows:

- A novel DCM is proposed considering the mapping relationship between physical environment features and electromagnetic propagation mechanisms. The DCM can provide accurate channel information and channel characteristics within a specific geographic area, and most importantly, update the map data in real-time as the physical environment changes.
- To ensure that the DCM can provide accurate channel characteristics while maintaining time-efficiency, we propose a novel stochastic-deterministic hybrid channel modeling structure for the DCM construction. The static interaction objects (IOs) are modeled offline by RT.

Meanwhile, MPCs of dyamic IOs are modeled and online updated by 6GPCM.

- We conduct a time-varying sub-6 GHz channel measurement, further implementing the proposed DCM of the measurement scenario based on the hybrid channel model. The accuracy of DCM is verified by comparing the root mean square (RMS) angular spread and RMS delay spread of synthetic channel with that of the measurement channel, RT channel, and 6GPCM.
- The time cost on updating the channel information of DCM is compared with the conventional channel map construction methods. The comparison result demonstrates the time-efficiency of DCM.

The rest of this paper is organized as follows. The novel stochastic-deterministic hybrid channel model for the construction of DCM is proposed in Section II. Section III gives a brief description of measurement configuration and data processing procedure. The validation and evaluation of DCM are given in Section IV. Finally, conclusions are drawn in Section V.

II. System Model

To construct an accurate and time-efficient DCM, a novel stochastic-deterministic hybrid channel model is proposed in this section. Note that to provide customized high-quality services for different 6G MIMO space-air-ground-sea wireless communication scenarios, DCM covers a specific geographic area including line-of-sight (LoS) and non-line-of-sight (NLoS) conditions, further adaptively provide diverse channel information within different communication scenarios. Consequently, we take a typical communication scenario containing static and dynamic IOs shown in Fig. 1 as an example, to illustrate the proposed channel model.

A. General Model Framework

The geometrical diagram of the proposed hybrid channel model is presented in Fig. 2. The numbers of antennas of the transmitter (Tx) and receiver (Rx) sides are denoted as M_T and M_R, respectively. A_q^T and A_p^R denote the qth $(q = 1, ..., M_T)$ and pth $(p = 1, ..., M_R)$ antenna of Tx and Rx. To describe the channel model clearly, only the kth $(k = 1, ..., K_{qp}(t))$ static scatterer and the nth $(n = 1, ..., N_{qp}(t))$ dynamic cluster are illustrated in Fig. 2, where $K_{qp}(t)$ is the number of static

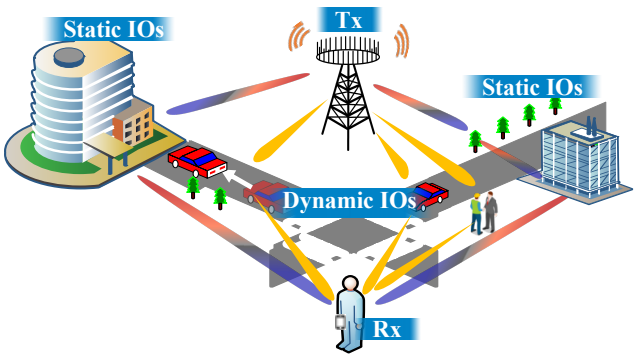

Fig. 1. Typical communication environment with static and dynamic IOs.

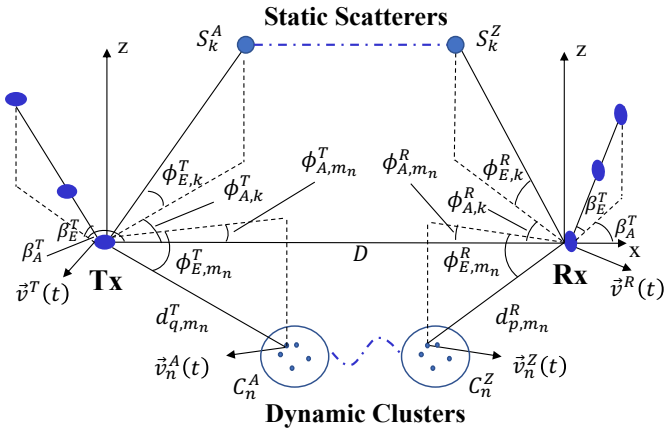

Fig. 2. Procedure of channel generation.

scatterer between A_q^T and A_p^R at moment t, $N_{qp}(t)$ is the number of dynamic cluster between A_q^T and A_p^R at moment t. Here, $K_{qp}(t)$ is time-varying because the motion of Tx and Rx. Considering the multi-bounce propagation, the nth dynamic cluster is denoted as cluster pairs, including the first-bounce cluster C_n^A at Tx side and the last-bounce cluster C_n^Z at Rx side. The mth $(m = 1, ..., M_n)$ ray in C_n^A is also illustrated in Fig. 2, where M_n represents the total number of rays in C_n^A. For the static IOs in physical environment, LoS and specular contributions are considered as two major wave propagation mechanisms, and the MPCs based on the LoS and specular contributions are defined as static scattering MPC. Here, the specular contributions include reflection, penetration, and diffraction components. The propagation through the kth static scattering MPC is modeled as a deterministic channel model and is denoted as scatterer pairs. The proposed hybrid channel model parameters are summarized in Table I. $h_{qp}(t, \tau)$ is defined as the channel impulse response (CIR) between A_q^T and A_p^R and can be expressed as the sum of the static component and dynamic component

$$h_{qp}(t,\tau) = \sqrt{\frac{K_R}{K_R+1}} h_{qp}^S(t,\tau) + \sqrt{\frac{1}{K_R+1}} h_{qp}^D(t,\tau), \quad (1)$$

where h_{qp}^S and h_{qp}^D denote the static component and dynamic component, respectively. K_R denotes the Rician factor, which is the ratio of the power of LoS components to the power of NLoS components. The CIRs of static channel and dynamic channel will be introduced in the next two subsections.

B. Static CIR

For the static environment, the RT geometric-optic method is used to generate the LoS path and the MPCs of static scatterers in physical environment, such as buildings, trees, and ground. The RT method can analyze the electromagnetic propagation process accurately and produce the parameters of MPCs. The static CIR in (1) can be calculated as

$$h_{qp}^S(t,\tau) = h_{qp}^{S-LoS}(t,\tau) + h_{qp}^{S-NLoS}(t,\tau), \quad (2)$$

where $h_{qp}^{S-LoS}(t, \tau)$ and $h_{qp}^{S-NLoS}(t, \tau)$ denote the LoS component and NLoS component of static CIR, respectively.

TABLE I
DEFINITIONS OF PARAMETERS IN THE STOCHASTIC-DETERMINISTIC HYBRID CHANNEL MODEL.

Parameters	Definitions
S_k^A, S_k^Z	The first and last bounce of the kth static scatterer at Tx and Rx
$S_{m_n}^A, S_{m_n}^Z$	The mth scatterer in C_n^A / C_n^Z
$\beta_{E/A}^T, \beta_{E/A}^R$	The elevation / azimuth angle of the Tx and Rx antenna array
$\alpha_{E/A}^T(t), \alpha_{E/A}^R(t)$	The elevation / azimuth angle of moving direction of Tx and Rx at time instant t
$\alpha_{E/A}^{A_n}(t), \alpha_{E/A}^{Z_n}(t)$	The elevation / azimuth angle of moving direction of C_n^A and C_n^Z at time instant t
$\phi_{E/A,k}^T, \phi_{E/A,k}^R$	The elevation / azimuth angle of departure and arrival of S_k^A and S_k^Z at initial moment
$\phi_{E/A,L}^T, \phi_{E/A,L}^R$	The elevation / azimuth angle of departure and arrival of the LoS path at initial moment
$\phi_{E/A,m_n}^T, \phi_{E/A,m_n}^R$	The elevation / azimuth angle of departure and arrival of $S_{m_n}^A$ and $S_{m_n}^Z$ at initial moment
$v^T(t), v^R(t)$	The absolute value of the velocity of Tx and Rx at time instant t
$v_n^A(t), v_n^Z(t)$	The absolute value of the velocity of C_n^A and C_n^Z at time instant t
$d_{m_n}^T, d_{m_n}^R$	Distance between A_1^T and $S_{m_n}^A$ / A_1^R and $S_{m_n}^Z$ at initial moment

The calculations of $h_{qp}^{S-LoS}(t,\tau)$ and $h_{qp}^{S-NLoS}(t,\tau)$ can be expressed as (3) and (4) shown at the bottom of this page.

Here, $\{\cdot\}^{\mathrm{T}}$ denotes the transposition operation, $F_{p/q,V(H)}$ stand for the vertical (horizontal) polarization of A_q^T / A_p^R. $\kappa_k(t)$ is the cross polarization power ratio, μ is co-polar imbalance [15], θ_L^{VV}, θ_L^{VH}, θ_k^{VV}, θ_k^{VH}, θ_k^{HV}, and θ_k^{HH} are the initial phases uniformly distributed between $[0, 2\pi]$. f_c denotes carrier frequency. In (4), $P_{qp,k}(t)$ and $\tau_{qp,k}(t)$ are the power and propagation delay of the kth ray between antenna A_q^T and A_p^R at time instant t. Paramaters in (4) mentioned above can be obtained in RT simulator.

When it comes to the LoS components in (3), $\tau_{qp}^L(t)$ denotes the propagation delay of the LoS path and can be obtained by RT simulation.

C. Dynamic CIR

To efficiently characterize the dynamic IOs in physical environment, dynamic scattering channel is modeled by 6GPCM, which can provide pervasiveness, applicability and time-efficiency for the proposed DCM. Noting that only NLoS path is considered in dynamic scattering channel, the expression is illustrated at the bottom of the next page [5]. Here, $\kappa_k(t)$ is the cross-polarization power ratio. $\theta_{m_n}^{VV}$, $\theta_{m_n}^{VH}$, $\theta_{m_n}^{HV}$, and $\theta_{m_n}^{HH}$ are the initial phases uniformly distributed between $[0, 2\pi]$. $P_{qp,m_n}(t)$ and $\tau_{qp,m_n}(t)$ are the power and propagation delay of the kth ray between antenna A_q^T and A_p^R at time instant t, where $\tau_{qp,m_n}(t)$ can be calculated as [5]

$$\tau_{qp,m_n}(t) = \frac{d_{q,m_n}^T(t) + d_{p,m_n}^R(t)}{c} + \tilde{\tau}_{m_n}, \tag{6}$$

where c denotes the speed of light in free space, $\tilde{\tau}_{m_n}$ denotes the delay of virtual link between $C_{m_n}^A$ and $C_{m_n}^Z$, $d_{q,m_n}^T(t)$ and $d_{p,m_n}^R(t)$ denote the distance of antenna A_q^T and scatterer $S_{m_n}^A$ and the distance of antenna A_p^R and scatterer $S_{m_n}^Z$ at time instant t. They can be modeled as [5]

$$\tilde{\tau}_{m_n} = \frac{\tilde{d}_{m_n}}{\tau_{C,link}} \tag{7}$$

$$h_{qp}^{S-LoS}(t,\tau) = \begin{bmatrix} F_{p,V}\left(\phi_{E,L}^R(t), \phi_{A,L}^R(t)\right) \\ F_{p,H}\left(\phi_{E,L}^R(t), \phi_{A,L}^R(t)\right) \end{bmatrix}^{\mathrm{T}} \begin{bmatrix} e^{j\theta_L^{VV}} & 0 \\ 0 & e^{j\theta_L^{HH}} \end{bmatrix} \begin{bmatrix} F_{q,V}\left(\phi_{E,L}^T(t), \phi_{A,L}^T(t)\right) \\ F_{q,H}\left(\phi_{E,L}^T(t), \phi_{A,L}^T(t)\right) \end{bmatrix} e^{j2\pi f_c \tau_{qp}^L(t)} \cdot \delta\left(\tau - \tau_{qp}^L(t)\right) \tag{3}$$

$$h_{qp}^{S-NLoS}(t,\tau) = \sum_{k=1}^{K_{qp}(t)} \begin{bmatrix} F_{p,V}\left(\phi_{E,k}^R(t), \phi_{A,k}^R(t)\right) \\ F_{p,H}\left(\phi_{E,k}^R(t), \phi_{A,k}^R(t)\right) \end{bmatrix}^{\mathrm{T}} \begin{bmatrix} e^{j\theta_k^{VV}} & \sqrt{\mu\kappa_k^{-1}(t)}e^{j\theta_k^{VH}} \\ \sqrt{\kappa_k^{-1}(t)}e^{j\theta_k^{HV}} & \sqrt{\mu}e^{j\theta_k^{HH}} \end{bmatrix} \begin{bmatrix} F_{q,V}\left(\phi_{E,k}^T(t), \phi_{A,k}^T(t)\right) \\ F_{q,H}\left(\phi_{E,k}^T(t), \phi_{A,k}^T(t)\right) \end{bmatrix} \sqrt{P_{qp,k}(t)} \cdot e^{j2\pi f_c \tau_{qp,k}(t)} \cdot \delta\left(\tau - \tau_{qp,k}(t)\right) \tag{4}$$

$$h_{qp}^{D}(t,\tau) = \sum_{n=1}^{N_{qp}(t)} \sum_{m=1}^{M_n} \begin{bmatrix} F_{p,V}\left(\phi_{E,m_n}^R(t), \phi_{A,m_n}^R(t)\right) \\ F_{p,H}\left(\phi_{E,m_n}^R(t), \phi_{A,m_n}^R(t)\right) \end{bmatrix}^{\mathrm{T}} \begin{bmatrix} e^{j\theta_{mn}^{VV}} & \sqrt{\mu\kappa_{m_n}^{-1}(t)}e^{j\theta_{mn}^{VH}} \\ \sqrt{\kappa_{m_n}^{-1}(t)}e^{j\theta_{mn}^{HV}} & \sqrt{\mu}e^{j\theta_{mn}^{HH}} \end{bmatrix} \begin{bmatrix} F_{q,V}\left(\phi_{E,m_n}^T(t), \phi_{A,m_n}^T(t)\right) \\ F_{q,H}\left(\phi_{E,m_n}^T(t), \phi_{A,m_n}^T(t)\right) \end{bmatrix} \sqrt{P_{qp,m_n}(t)} \cdot e^{j2\pi f_c \tau_{qp,m_n}(t)} \cdot \delta\left(\tau - \tau_{qp,m_n}(t)\right) \tag{5}$$

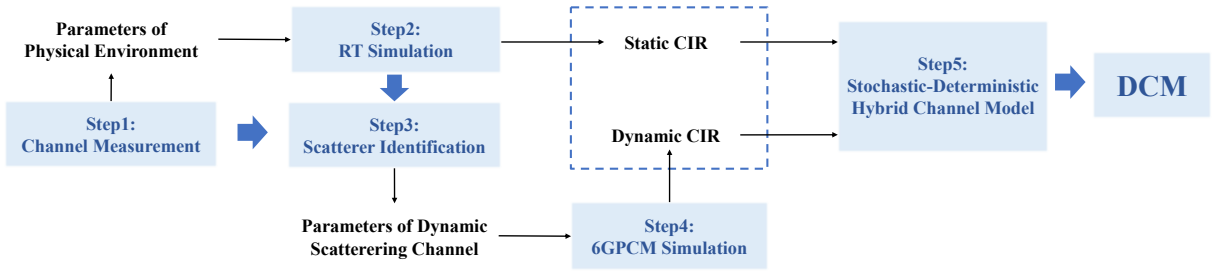

Fig. 3. Procedure of DCM construction based on stochastic-deterministic hybrid channel model.

and

$$\begin{aligned} d^T_{q,m_n}(t) &= ||\vec{d}^T_{m_n} - [\vec{l}^T_q + \int_0^t \vec{v}^T(t) - \vec{v}^A_n(t)dt]|| \\ d^R_{p,m_n}(t) &= ||\vec{d}^R_{m_n} - [\vec{l}^R_p + \int_0^t \vec{v}^R(t) - \vec{v}^Z_n(t)dt]||. \end{aligned} \tag{8}$$

In (7), $\tau_{C,link}$ is a non-negative variable randomly generated according to the exponential distribution. In (8), $\vec{d}^T_{m_n}$ denotes the vector pointing from A^T_1 to $S^A_{m_n}$ and $\vec{d}^R_{m_n}$ denotes the vector pointing from A^R_1 to $S^Z_{m_n}$ at the initial moment. They are calculated as

$$\begin{aligned} \vec{d}^T_{m_n} =& d^T_{m_n} \cdot [\cos\phi^T_{E,m_n}\cos\phi^T_{A,m_n}, \\ & \cos\phi^T_{E,m_n}\sin\phi^T_{A,m_n}, \sin\phi^T_{E,m_n}] \end{aligned} \tag{9}$$

$$\begin{aligned} \vec{d}^R_{m_n} =& d^R_{m_n} \cdot [\cos\phi^R_{E,m_n}\cos\phi^R_{A,m_n}, \\ & \cos\phi^R_{E,m_n}\sin\phi^R_{A,m_n}, \sin\phi^R_{E,m_n}]. \end{aligned} \tag{10}$$

In (8), $\vec{v}^T(t)$, $\vec{v}^R(t)$, $\vec{v}^A_n(t)$, and $\vec{v}^Z_n(t)$ are the vectors of the velocities of Tx, Rx, C^A_n, and C^Z_n. They are expressed as

$$\begin{aligned} \vec{v}^X(t) =& v^X(t)[\cos\alpha^X_E(t)\cos\alpha^X_A(t), \\ & \cos\alpha^X_E(t)\sin\alpha^X_A(t), \sin\alpha^X_E(t)], \end{aligned} \tag{11}$$

where $X = \{T, R, A_n, Z_n\}$.

l^T_q and l^R_p in (8) denote the vector pointing from A^T_1 to A^T_q and the vector pointing from A^R_1 to A^R_p, respectively. They are expressed as

$$\vec{l}^T_q = \delta_q \cdot [\cos\beta^T_E\cos\beta^T_A, \cos\beta^T_E\sin\beta^T_A, \sin\beta^T_E] \tag{12}$$

$$\vec{l}^R_p = \delta_p \cdot [\cos\beta^R_E\cos\beta^R_A, \cos\beta^R_E\sin\beta^R_A, \sin\beta^R_E], \tag{13}$$

where the variable δ_q and δ_p in (12) and (13) represent the distance from A^T_q to A^T_1 and the distance from A^R_q to A^R_1. They can be calculated as $\delta_q = (q-1)\delta^T$ and $\delta_p = (p-1)\delta^R$, where δ^T and δ^R denote the antenna interval of Tx and Rx, respectively.

III. Model Implementation

In this section, we conduct a sub-6 GHz channel measurement containing static and dynamic IOs and implement the proposed stochastic-deterministic hybrid channel model of the measurement scenario. The static scattering channel is modeled by RT method. By matching the MPCs between static scattering channel and estimated real channel by the space-alternating generalized expectation maximization (SAGE) algorithm, DCM for this area is constructed. The detailed procedure of the model implementation is shown in Fig. 3.

TABLE II
System Setup.

Parameters	Configurations
Carrier frequency (GHz)	5.5
Bandwidth (MHz)	320
Rx antenna array	8×8 dual-polarization cylindrical antenna array
Tx antenna array	single omnidirectional antenna
PN code length (chips)	1023
Transmit power (dBm)	40
Length of sounding signal	4us

A. Channel Measurement Campaign

The measurement campaign was carried out using the Keysight time-domain channel sounder, comprising a Tx side and a Rx side. The center frequency of the transmission signal is 5.5 GHz, and the bandwidth is 320 MHz. The transmitting antenna is a single omnidirectional antenna, and the receiving antenna is an 8×8 dual-polarization cylindrical antenna array. The measurements were conducted at the ChinaNetwork Valley site in Nanjing, China, where four office buildings are about 37 meters high.

Each building is separated by approximately 60 meters, and the venue is covered with vegetation. The single omnidirectional antenna at the Tx side is fixed on a metal stand and placed on the eighth floor of an office building at a height of 30 meters. The antenna array at the Rx side is attached to a trolley and moves on different routes within the venue. This measurement campaign includes LoS and NLoS routes. NLoS propagation is mostly caused by the obstruction of buildings. The detailed measurement routes are shown in Fig. 4. Measurement positions are uniformly distributed across all routes. Detailed system configurations are summarized in Table II. Using the high-resolution SAGE algorithm [16], the MPCs are then extracted from the measurement results.

B. Ray Tracing Simulation

As shown in Fig. 5, we reconstruct the scenario of China Valley using Wireless Insite (WI), a wireless propagation software. Here, we take propagation mechanisms, LoS and reflections into account. We select up to sixth order of reflection to obtain tractable computational complexity for RT. To obtain the parameters of static channels, only static IOs in environment including buildings and trees are setting in WI.

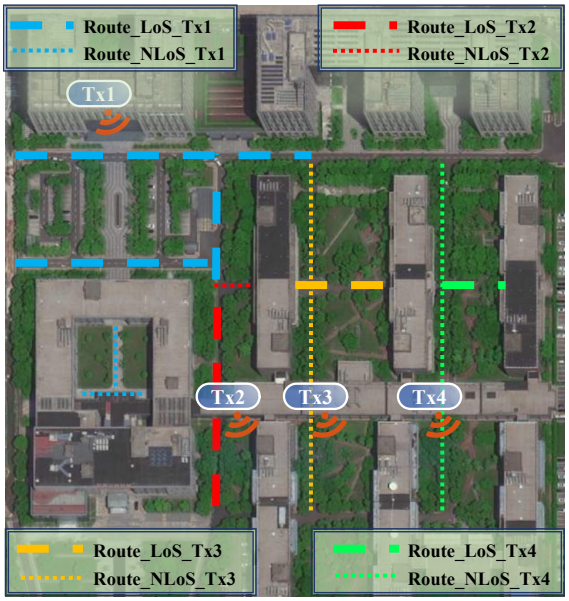

Fig. 4. Overview of the measurement scenario and deployment.

C. MPC Matching between RT and Measurement

Based on the parameters estimated by SAGE algorithm and the parameters of rays in RT simulation, the MPCs in RT channel (RT-MPCs) and MPCs in measured channel (M-MPCs) can be illustrated in the joint azimuth angle of arrival (AAoA) and delay domain as shown in Fig. 6, where each marker deontes one MPC. Colors of the symbols indicate the power of the corresponding MPCs. A RT-MPC are considered to be matched with a M-MPC if the Euclidean distance between them is smaller than a defined threshold. The matching MPCs are labeled with red dotted circles and other MPCs are labeled with pink solid circles, standing for the dynamic clusters. It can be found from Fig. 6 that each RT-MPC can be matched with at least one M-MPC and the power of matching MPCs is almost the same. However, there are still some observable M-MPCs, which cannot be matched with RT-MPCs. Because the dynamic IOs in physical environment are not considered in RT simulation, these M-MPCs may be caused by diffraction and diffuse scattering from dynamic IOs, corresponding to the dynamic clusters in the proposed stochastic-deterministic hybrid channel model.

By matching the M-MPCs with different IOs in physical environment, we can obtain the value of K_{qp} and $N_{qp}(t)$ in simulation setting of the proposed hybrid model, which can be further used in the accuracy evaluation to ensure a fair comparison.

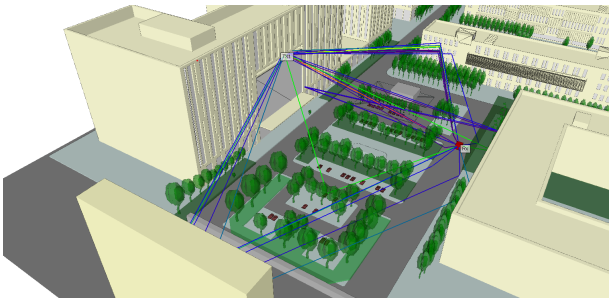

Fig. 5. RT simulation scenario reconstructed in WI.

IV. Validation and Evaluation

A. Accuracy Evaluation

Due to the randomness of wireless channels, it is inappropriate to evaluate the channel model by comparing the generated CIR with the measured data directly. As a feasible method, the statistical properties of wireless channels can be used instead to validate the effectiveness in a stochastic way. In this work, the accuracy of DCM is verified by validating the effectiveness of the proposed hybrid channel model.

The CDFs of RMS angular spread and RMS delay spread of the proposed hybrid channel model, channel measurement, RT, and 6GPCM are compared in Fig. 7. We can see from Fig. 7 that the RMS angular spread and RMS delay spread of the proposed hybrid channel model, RT method, and 6GPCM all accord well with the measurement results. This indicates that the proposed model achieves good model accuracy.

B. Time-Efficiency

As the physical environment changes, channel map should be updated. To validate the generation efficiency of DCM, the computation time is compared under the scenario of Fig. 4 on a computer with Intel Xeon CPU E5 and 16 GB RAM. The RT algorithm consumes 1.2 hour to track and

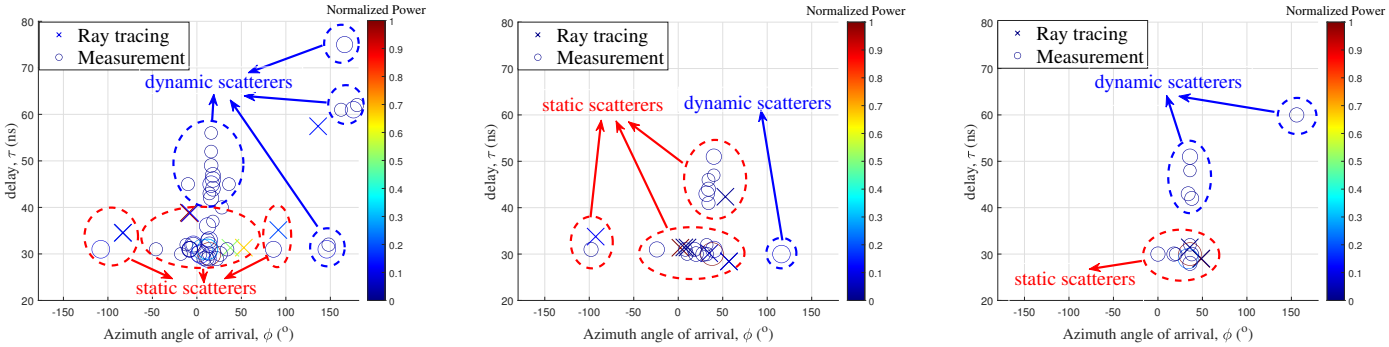

Fig. 6. Normalized AAoA-delay PSD of RT and measurement in Route_LoS_Tx1 (a) location 3, (b) location 7, and (c) location 9.

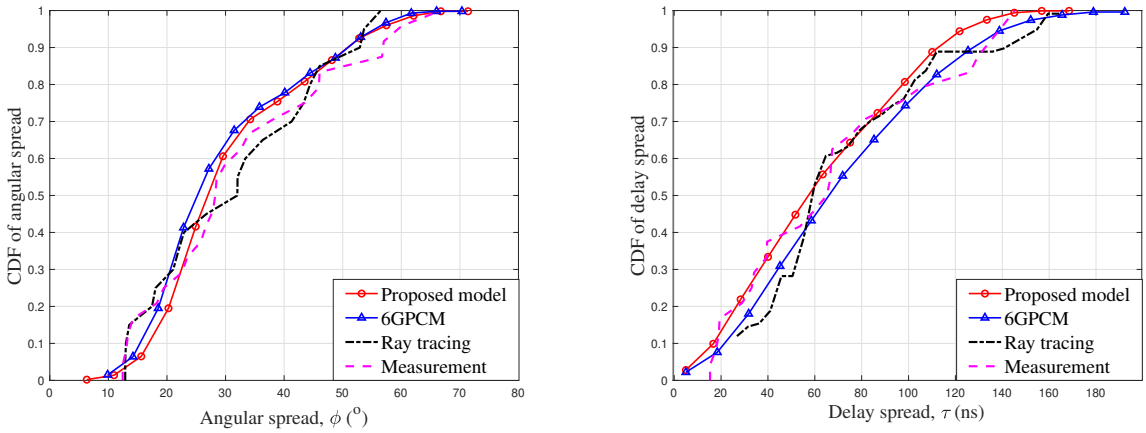

(a) (b)

Fig. 7. CDFs of (a) RMS angular spread and (b) RMS delay spread of the proposed hybrid channel model, channel measurement, RT, and 6GPCM.

calculate all parameters of 120 rays. However, the proposed hybrid channel model only takes 1.4 seconds to generate the dynamic CIR. Consequently, if the physical environment changes per minute, conventional channel maps constructed by instantaneous channel measurement/RT method cannot update the pre-store data, but the DCM can provide valid channel information in 2 seconds.

V. Conclusions

In this paper, a novel DCM for 6G MIMO communications has been proposed. To construct the DCM accurately and time-efficiently, we have developed a stochastic-deterministic hybrid channel model, where the static and dynamic IOs in physical environment are model by RT method and 6GPCM, respectively. Furthermore, based on channel measurement, DCM in this area has been implemented by using the proposed channel model. To validate the accuracy of DCM, the RMS angular spread, RMS delay spread, and computation time for DCM online update have been compared between the synthetic channel, measured channel, RT results, and 6GPCM. The results have shown that the proposed DCM construction method is as accurate as RT and 6GPCM, while comsuming less time on updating than conventional channel maps constructed by RT method or instantaneous channel measurements when the physical environment changes.

VI. Acknowledgment

This work was supported by the National Key R&D Program of China under Grants 2023YFB2904802, the Fundamental Research Funds for the Central Universities under Grant 2242022k60006, the National Natural Science Foundation of China (NSFC) under Grants 62394290, 62394291, 61960206006, 62301364, and 62301151, the Key Technologies R&D Program of Jiangsu (Prospective and Key Technologies for Industry) under Grants BE2022067 and BE2022067-1, the Research Fund of National Mobile Communications Research Laboratory, Southeast University, under Grant 2024A05, the Young Elite Scientists Sponsorship Program by China Association for Science and Technology (CAST) (2022QNRC001), and the Start-up Research Fund of Southeast University under Grant RF1028623062.

References

[1] X. You, *et al.*, "Towards 6G wireless communication networks: Vision, enabling technologies, and new paradigm shifts," *Science China Information Sciences*, vol. 64, no. 1, Jan. 2021.

[2] C. -X. Wang, *et al.*, "On the road to 6G: Visions, requirements, key technologies, and testbeds," *IEEE Commun. Surveys Tut.*, vol. 25, no. 2, pp. 905–974, 2nd quart. 2023.

[3] C. -X. Wang, J. Huang, H. Wang, X. Gao, X. You, and Y. Hao, "6G wireless channel measurements and models: Trends and challenges," *IEEE Veh. Technol. Mag.*, vol. 15, no. 4, pp. 22–32, Dec. 2020.

[4] C. A. Balanis, *Advanced engineering electromagnetics (second edition)*, Hoboken: John Wiley, 2012.

[5] C. -X. Wang, Z. Lv, X. Gao, X. You, Y. Hao, and H. Haas, "Pervasive wireless channel modeling theory and applications to 6G GBSMs for all frequency bands and all scenarios," *IEEE Trans. Veh. Technol.*, vol. 71, no. 9, pp. 91599173, Sept. 2022.

[6] C. -X. Wang, Z. Lv, Y. Chen, and H. Haas, "A complete study of space-time-frequency statistical properties of the 6G pervasive channel model," *IEEE Trans. Commun.*, vol. 71, no. 12, pp. 7273–7287, Dec. 2023.

[7] C. Huang, R. Wang, C. -X. Wang, P. Tang, and A. F. Molisch, "A geometry-based stochastic model for truck communication channels in freeway scenarios," *IEEE Trans. Commun.*, vol. 70, no. 8, pp. 5572–5586, Aug. 2022.

[8] Y. Zeng and X. Xu, "Toward environment-aware 6G communications via channel knowledge map," *IEEE Wireless Commun.*, vol. 28, no. 3, pp. 84–91, June 2021.

[9] K. Li, P. Li, Y. Zeng, and J. Xu, "Channel knowledge map for environment-aware communications: EM algorithm for map construction," in *Proc. IEEE WCNC'22*, Austin, TX, USA, 2022, pp. 1659–1664.

[10] Y. Long, Y. Zeng, X. Xu, and Y. Huang, "Environment-aware wireless localization enabled by channel knowledge map," in *Proc. IEEE GC'22*, Rio de Janeiro, Brazil, 2022, pp. 5354–5359.

[11] C. A. Oroza, Z. Zhang, T. Watteyne, and S. D. Glaser, "A machine-learning-based connectivity model for complex terrain large-scale low-power wireless deployments," *IEEE Trans. Cogn. Commun. Netw.*, vol. 3, no. 4, pp. 576–584, Dec. 2017.

[12] K. Suto, *et al.*, "Image-driven spatial interpolation with deep learning for radio map construction," *IEEE Wireless Commun. Lett.*, vol. 10, no. 6, pp. 1222–1226, June 2021.

[13] K. Katagiri, K. Sato, K. Inage, and T. Fujii, "Radio map extrapolation using compensated empirical CDF under interference-limited observations," *IEEE Access*, vol. 10, pp. 54936–54946, May 2022.

[14] C. E. G. Moreta, M. R. C. Acosta, and I. Koo, "Prediction of digital terrestrial television coverage using machine learning regression," *IEEE Trans. Broadcast.*, vol. 65, no. 4, pp. 702–712, Dec. 2019.

[15] J. Bian, C.-X. Wang, X.-Q. Gao, X.-H. You, and M. Zhang, "A general 3D non-stationary wireless channel model for 5G and beyond," *IEEE Trans. Wireless Commun.*, vol. 20, no. 5, pp. 3211–3224, May 2021.

[16] B. H. Fleury, M. Tschudin, R. Heddergott, D. Dahlhaus, and K. Ingeman Pedersen, "Channel parameter estimation in mobile radio environments using the SAGE algorithm," *IEEE J. Sel. Areas Commun.*, vol. 17, no. 3, pp. 434–450, Mar. 1999.